Solid-State Electronics 67 (2012) 105–108

Contents lists available at ScienceDirect

Solid-State Electronics

journal homepage: www.elsevier.com/locate/sse

High-frequency, 6.2 Å *pN* heterojunction diodes

James G. Champlain *, Richard Magno, Doewon Park, Harvey S. Newman, J. Brad Boos

Electronics Science and Technology Division, Naval Research Laboratory, Washington, DC 20375, USA

ARTICLE INFO

Article history:
Received 19 May 2011
Accepted 19 July 2011
Available online 8 September 2011

The review of this paper was arranged by Prof. A. Zaslavsky

Keywords:
Semiconductor devices
Diodes
Mixers
Frequency conversion

ABSTRACT

Sb-based *pN* heterojunction diodes at 6.2 Å, consisting of narrow bandgap *p*-type $In_{0.27}Ga_{0.73}Sb$ and wide bandgap *n*-type $In_{0.69}Al_{0.41}As_{0.41}Sb_{0.59}$, have been fabricated and measured. These diodes show excellent electrical characteristics with an ideality factor of 1.2 and high current density. *S*-parameter measurements and subsequent analysis show that these diodes have *RC*-cutoff frequencies over 1 THz, making these diodes excellent choices for high-frequency applications, such as sub-harmonic mixers for frequency conversion.

Published by Elsevier Ltd.

1. Introduction

The 6.1 Å materials, as they are commonly referred to, InAs, AlSb, GaSb, and their alloys (e.g., $In_{0.2}Al_{0.8}Sb$, $InAs_{0.9}Sb_{0.1}$) have become highly desirable for use in low-power, high-speed electronic applications due to a large range of available bandgaps and band offsets and high electron and hole mobilities. High electron mobility transistors (HEMTs) fabricated from these materials have shown good operating characteristics [1,2]. Furthermore, the first monolithic microwave integrated circuits (MMICs) fabricated using 6.1 Å based HEMTs have been demonstrated [3]. New materials such as $In_xGa_{1-x}Sb$, $InAs_ySb_{1-y}$, and $In_xAl_{1-x}As_ySb_{1-y}$, with lattice constants ranging from 6.1 Å to 6.48 Å, show promise of further power reduction, due to narrower bandgaps, while maintaining or possibly improving high-speed operation [4]. These new materials' potential has been already demonstrated in HEMTs [5,6], diodes [7], and heterojunction bipolar transistors (HBTs) [8] at lattice constants around 6.2 Å. Additionally, increased interest in imaging technology in the sub-terahertz to terahertz (THz) frequency range [9–11], especially in limited power applications, has resulted in further examination of these materials for devices needed to produce high-frequency mixers and multipliers.

For frequency conversion, traditionally anti-parallel Schottky diode pairs have been used as sub-harmonic mixers. Schottky diodes have been preferable over *pn* diodes due to the latter's relatively higher overall capacitance and subsequently reduced frequency performance. The higher capacitance seen in *pn* diodes is explained as due to the addition of a diffusion capacitance associated with the diffusion of excess minority carriers within the neutral bulk of the device. Restriction to the use of Schottky diodes limits the fabrication of these devices to relatively larger bandgap materials (e.g., GaAs), as simple Schottky contacts to narrower bandgap materials (e.g., InAs) are practically impossible.

However, the work by Laux and Hess suggests that diffusion capacitance in *pn* diodes is not nearly as high as previously believed [12]. Additionally, *pn* diodes can effectively function as unipolar devices by "removing" one carrier type by means of a heterostructure barrier (e.g., $\Delta\mathcal{E}_v$ greater than a few *kT* blocks hole injection). The end result is a greatly reduced diffusion capacitance for the heterojunction *pn* diode and subsequently improved frequency performance. Therefore, heterojunction *pn* diodes fabricated from 6.1 to 6.3 Å materials are expected to exceed the performance of current state-of-the-art GaAs Schottky diodes.

In this letter, MMIC-compatible Sb-based *pN* heterojunction diodes at a lattice constant of $a = 6.2$ Å, consisting of narrow bandgap *p*-type $In_{0.27}Ga_{0.73}Sb$ and wide bandgap *n*-type $In_{0.69}Al_{0.41}As_{0.41}Sb_{0.59}$, are presented that show excellent electrical behavior with *RC*-cutoff frequencies (f_{RC}) exceeding 1 THz.

2. Materials and methods

The *pN* diodes presented in this paper were grown by solid-source molecular beam epitaxy (MBE). Here, the use of a lower-case letter (*p*) for the narrow bandgap layer and upper-case letter (*N*) for the wide bandgap layer follows that established by Kroemer [13,14]. Beginning with a semi-insulating (SI) GaAs substrate, the growth buffer consisted of 1000 Å unintentionally doped (UID)

* Corresponding author.
E-mail address: james.champlain@nrl.navy.mil (J.G. Champlain).

0038-1101/$ - see front matter Published by Elsevier Ltd.
doi:10.1016/j.sse.2011.07.010

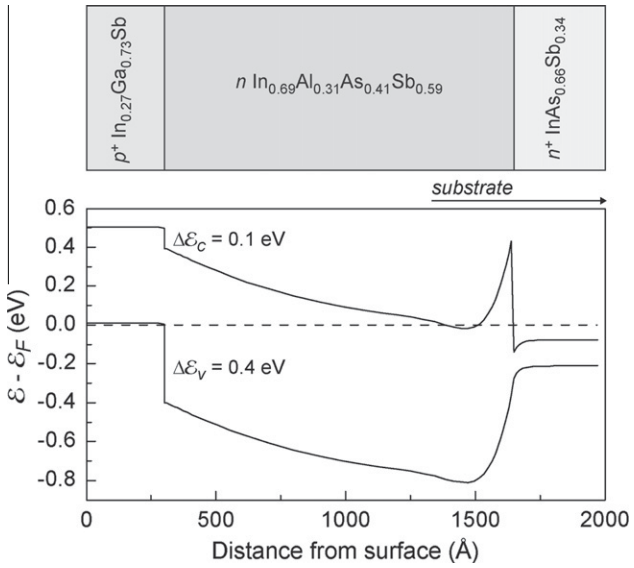

Fig. 1. Layer structure and band diagram of the *pN* diode examined in this paper. Bandgaps and band offsets are calculated following the work of Vurgaftman et al. [15]. The band diagram was simulated using ATLAS by SILVACO International.

GaAs (a = 5.65 Å), 5000 Å UID $Al_{0.65}Ga_{0.35}Sb$ (a = 6.12 Å), and 1 μm UID $In_{0.21}Ga_{0.19}Al_{0.60}Sb$ (a = 6.2Å). After the buffer, the growth was continued with a 5000 Å n^+ (Te: 3×10^{18} cm^{-3}) $InAs_{0.66}Sb_{0.34}$ contact layer; a $In_{0.69}Al_{0.31}As_{0.41}Sb_{0.59}$ wide bandgap n-layer consisting of an initial 50 Å n^+ (Te: 4×10^{18} cm^{-3}) layer, a 250 Å n-type doping grade (Te: 4×10^{18} to 5×10^{16} cm^{-3}), a 1000 Å n (Te: 5×10^{16} cm^{-3}) "bulk" layer, and a 50 Å UID spacer; and a 300 Å p^+ (Be: 3×10^{19} cm^{-3}) $In_{0.27}Ga_{0.73}Sb$ layer (Fig. 1).

$InAs_{0.66}Sb_{0.34}$ and $In_{0.27}Ga_{0.73}Sb$ were selected for the n-type contact and p-type contact layers, respectively, due to the excellent transport ($\mu_{n,InAsSb}$ = 5600 cm^2/Vs, $\mu_{p,InGaSb}$ = 160 cm^2/Vs) and contact ($r_{c,n\text{-}InAsSb} = 2.4 \times 10^{-8}\ \Omega\,\text{cm}^2$, $r_{c,p\text{-}InGaSb} = 8.9 \times 10^{-8}\ \Omega\,\text{cm}^2$) properties both have shown [16,17]. The relatively large valence band offset ($\Delta\mathcal{E}_v \approx 0.3$ eV) between $In_{0.27}Ga_{0.73}Sb$ ($\mathcal{E}_g = 0.49$ eV) and $In_{0.69}Al_{0.31}As_{0.41}Sb_{0.59}$ ($\mathcal{E}_g = 0.83$ eV) effectively makes the diode a unipolar electron device by blocking hole injection from the p-type $In_{0.27}Ga_{0.73}Sb$ into the n-type $In_{0.69}Al_{0.31}As_{0.41}Sb_{0.59}$. Additionally, the use of a thin or "short" p-type layer reduces any capacitance associated with the diffusion of minority electrons across the layer.

Diode fabrication began with the definition and deposition of Pd:Pt:Au (100:50:2500 Å) unannealed, p-type ohmic contacts onto the p^+ $In_{0.27}Ga_{0.73}Sb$ layer using standard e-beam lithography and e-beam evaporation. After which diode mesas were etched down to the $InAs_{0.66}Sb_{0.34}$ contact layer by a $SiCl_4$-based reactive-ion etch (RIE), using lithographically-defined photoresist as the etch mask. Subsequently, Ti:Pt:Au (100:50:2500 Å) unannealed, n-type ohmic contacts were defined and deposited onto the n^+ $InAs_{0.66}Sb_{0.34}$ contact layer. Diodes were isolated down to the SI GaAs substrate with a H_3PO_4-based wet etch. Diode fabrication was completed with a RF-compatible co-planar waveguide (CPW) and airbridge, between the diode and CPW (Fig. 2). Both circular and rectangular diodes were fabricated with sizes down to $A_{circ} = \pi(5/2)^2\ \mu\text{m}^2 \approx 20\ \mu\text{m}^2$ and $A_{rect} = 2 \times 5\ \mu\text{m}^2 = 10\ \mu\text{m}^2$, respectively.

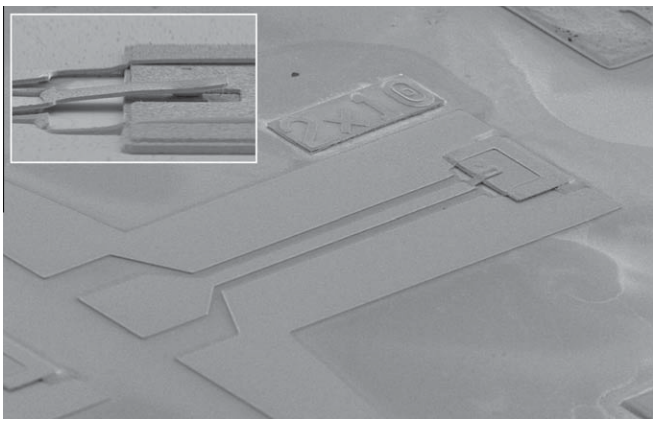

Fig. 2. Scanning electron microscope (SEM) image of a *pN* diode, including the co-planar wavequide (CPW). The inset shows a magnified view of the diode and bridge.

3. Measurements and discussion

Two-point current–voltage (*JV*) measurements on the diodes show excellent behavior with an ideality factor of $\eta \approx 1.2$, strong rectifying behavior, and area-dependent scaling (Fig. 3). As can be seen in the figure, the diodes do not become resistively limited until $V \approx V_{bi}$ = 0.39 V, suggesting that the series resistance of these diodes is very small.

One-port scattering parameter (*S*-parameter) measurements were taken of the diodes. The RF probes were calibrated on a separate calibration substrate, with open and short waveguide standards measured on-wafer. The waveguide was designed to be nominally 50 Ω for the range of frequencies measured (10 MHz–40 GHz). S_{11} of the as-measured device (waveguide and diode) and de-embedded diode for a $1 \times 10\ \mu\text{m}^2$ area diode, at an applied voltage of 0 V, are shown in Fig. 4.

A small-signal model consisting of a parallel resistance (R_j) and capacitance (C_j), representative of the diode's junction, in series with a second resistance (R_S), representing any series resistance due to the neutral, undepleted bulk and contacts, was used in the extraction of the various device components (Fig. 5), with the total extracted junction capacitance being the combination of the depletion and diffusion capacitance ($C_j = C_{dep} + C_{diff}$).

Diodes in general are useful up to frequencies given by $f_{RC} = 1/2\pi R_S C_j$. At frequencies above f_{RC}, the junction capacitance effectively appears as a short, resulting in the diode appearing as a simple resistance with a value of R_S and the characteristic current–voltage relationship of the diode is lost. The small-signal model was applied to both the as-measured device and de-embedded diode *S*-parameters of various area diodes. The resultant *RC*-cutoff frequencies, $f_{RC} = 1/2\pi R_S C_j$, from the extracted component values are plotted in Fig. 6.

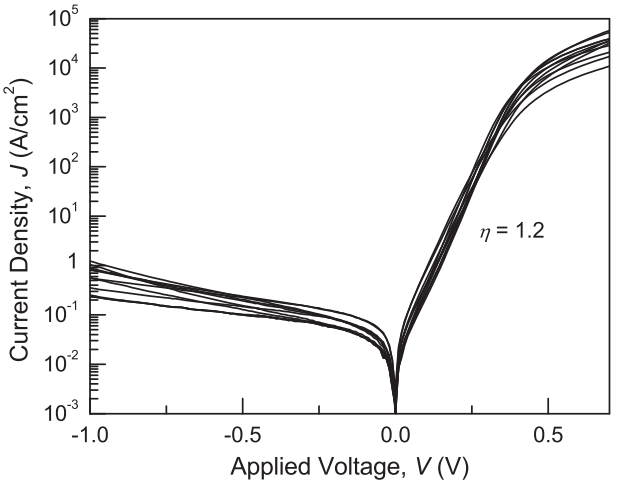

Fig. 3. Plot of the current–voltage (*JV*) measurements for circular and rectangular *pN* diodes of various area. The ideality factor for all measurements was $\eta \approx 1.2$.

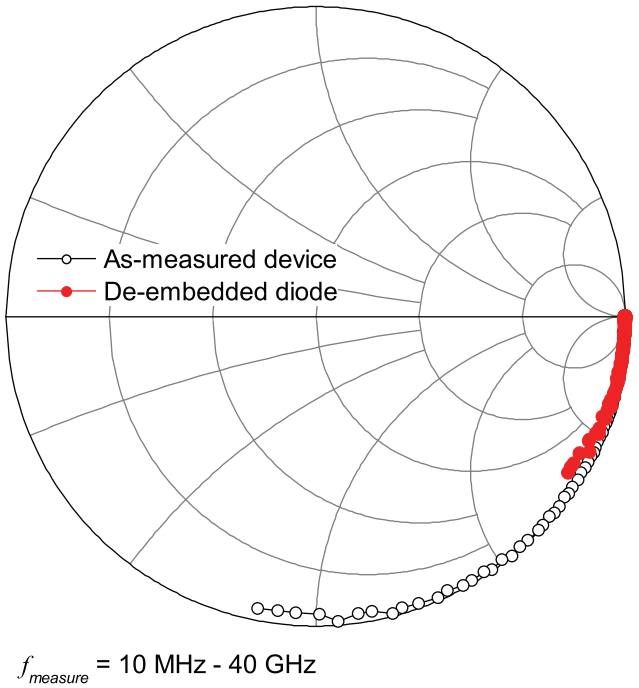

Fig. 4. S_{11} of the as-measured device (waveguide and diode, hollow symbols) and de-embedded diode (solid symbols) for a 1×10 μm^2 area diode, at an applied voltage of 0 V. The measurement frequency range was 10 MHz–40 GHz.

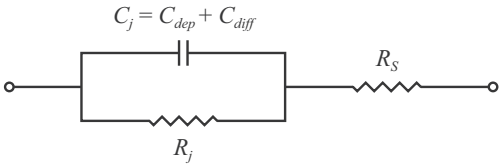

Fig. 5. Small-signal model of the *pN* diode. R_j and C_j represent the diode's junction resistance and capacitance, respectively, and R_S represents the total resistance outside of the junction due to the neutral, undepleted bulk and contacts.

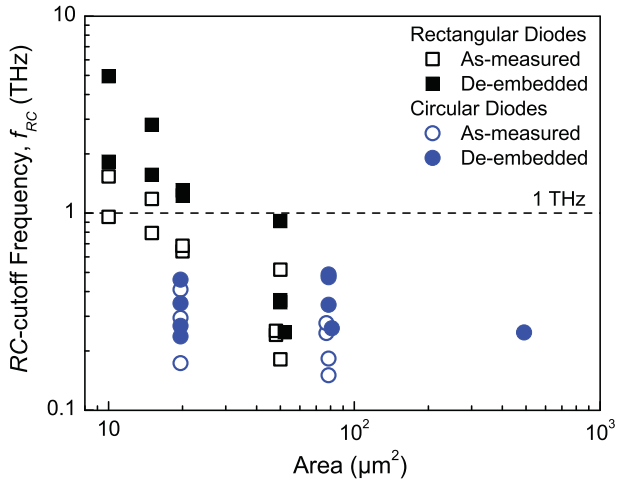

Fig. 6. Plot of the as-measured device and de-embedded diode *RC*-cutoff frequencies ($f_{RC} = 1/2\pi R_S C_j$) for circular and rectangular *pN* diodes of various area, calculated from the *S*-parameter extracted series resistance (R_S) and total junction capacitance (C_j). De-embedded diodes with an area $\leqslant$20 μm^2 exhibit $f_{RC} > 1$ THz. Note, overlapping points have been shifted for clarity.

As seen in the figure, even with the response of the waveguide included (hollow symbols), *pN* diodes with areas under 15 μm^2 have *RC*-cutoff frequencies over 1 THz. For de-embedded *pN* diodes with areas under 20 μm^2, *RC*-cutoff frequencies over 1 THz are observed (solid symbols, Fig. 6). Due to the limited frequency range used for the *S*-parameter measurements (10 MHz–40 GHz), accurate extraction of the the diode components, in particular R_S, for the smaller area diodes was difficult and requires higher frequency measurements to verify, but it is clear that f_{RC} exceeds 1 THz for these devices.

In general, rectangular diodes resulted in higher *RC*-cutoff frequencies, especially those with high *L*/*W* aspect ratios, as compared to circular diodes of similar area (Fig. 6). This is believed to be primarily due to the lower spreading resistance under the mesa for high *L*/*W* aspect ratio rectangular mesas ($R_{rect} = \rho_{sheet}/12 \times (L/W)^{-1}$, $R_{circ} = \rho_{sheet}/8\pi$)[18].

4. Conclusions

Sb-based *pN* heterojunction diodes at $a = 6.2$ Å, consisting of narrow bandgap, *p*-type $In_{0.27}Ga_{0.73}Sb$ and wide bandgap, *n*-type $In_{0.69}Al_{0.41}As_{0.41}Sb_{0.59}$, have been presented that show excellent electrical behavior ($\eta \approx 1.2$) with *RC*-cutoff frequencies (f_{RC}) exceeding 1 THz. This performance is a direct result of the excellent electronic properties (e.g., high mobility and low contact resistance) of $In_{0.27}Ga_{0.73}Sb$, $In_{0.69}Al_{0.31}As_{0.41}Sb_{0.59}$, and $InAs_{0.66}Sb_{0.34}$ and reduced capacitance associated with the *pN* heterojunction diode design.

Acknowledgement

This work was supported by the Office of Naval Research.

References

[1] Papanicolaou NA, Bennett BR, Boos JB, Park D, Bass R. Sb-based HEMTs with InAlSb/InAs heterojunction. Electron Lett 2005;41(19):1088–9.
[2] Bennett BR, Magno R, Boos JB, Kruppa W, Ancona MG. Antimonide-based compound semiconductors for electronic devices: a review. Solid-State Electron 2005;49(12):1875–95.
[3] Deal WR, Tsai R, Lange MD, Boos JB, Bennett BR, Gutierrez A. A w-band InAs/AlSb low-noise/low-power amplifier. IEEE Microw Wireless Compon Lett 2005;15(4):208–10.
[4] Magno R, Glaser ER, Tinkham BP, Champlain JG, Boos JB, Ancona MG, et al. InAlAsSb alloys for electronic devices. J Vacuum Sci Technol B 2006;24(3):1622–5.
[5] Boos JB, Bennett BR, Papanicolaou NA, Ancona MG, Champlain JG, Bass R, et al. High mobility p-channel HFETs using strained Sb-based materials. Electron Lett 2007;43(15):834–5.
[6] Boos JB, Bennett BR, Papanicolaou NA, Ancona MG, Champlain JG, Yeong-Chang C, et al. Sb-based n- and p-channel heterostructure FETs for high-speed, low-power applications. IEICE Trans Electron 2008;E91-C(7):050–1057.
[7] Champlain JG, Magno R, Doewon P, Newman HS, Boos JB. 6.2 Å Sb-based pN diodes for high frequency applications. In: 2007 Joint 32nd international conference on infrared and millimeter waves and the 15th international conference on terahertz electronics (IRMMW-THz); 2008. p. 855–6.
[8] Mairiaux E, Desplanque L, Wallart X, Zaknoune M. Microwave performance of InAlAsSb/$In_{0.35}Ga_{0.65}Sb$/InAlAsSb double heterojunction bipolar transistors. IEEE Electron Dev Lett 2010;31(4):299–301.
[9] Hu BB, Nuss MC. Imaging with terahertz waves. Opt Lett 1995;20(16):1716–8.
[10] van der Weide D. Applications and outlook for electronic terahertz technology. Opt Photon News 2003;14(4):48–53.
[11] Federici JF, Schulkin B, Feng H, Gary D, Barat R, Oliveira F, et al. THz imaging and sensing for security applications – explosives, weapons and drugs. Semicond Sci Technol 2005;20(7):S266–80.
[12] Laux SE, Hess K. Revisiting the analytic theory of p–n junction impedance: improvements guided by computer simulation leading to a new equivalent circuit. IEEE Trans Electron Dev 1999;46(2):396–412.
[13] Kroemer H, Chien W-Y, Harris Jr JS, Edwall DD. Measurement of isotype heretojunction barriers by C–V profiling. Appl Phys Lett 1979;36(4):295–7.
[14] Kroemer H. Analytic approximations for degenerate accumulation layers in semiconductors, with applications to barrier lowering in isotype heterojunctions. J Appl Phys 1980;52(2):873–8.

[15] Vurgaftman I, Meyer JR, Ram-Mohan LR. Band parameters for III–V compound semiconductors and their alloys. J Appl Phys 2001;89(11):5815–75.
[16] Champlain JG, Magno R, Boos JB. Low resistance, unannealed, ohmic contacts to p-type $In_{0.27}Ga_{0.73}Sb$. J Vacuum Sci Technol B (Microelectron Nanometer Struct) 2006;24(5):2388–90.
[17] Champlain JG, Magno R, Boos JB. Low resistance, unannealed ohmic contacts to n-type $InAs_{0.66}Sb_{0.34}$. Electron Lett 2007;43(23):1315–7.
[18] Phillips AB. Transistor engineering and introduction to integrated semiconductor circuits. McGraw-Hill series in solid-state engineering. New York: New McGraw-Hill Book Company; 1962.